Level-set method for island dynamics in epitaxial growth

C. Ratsch,[1,*] M. F. Gyure,[2] R. E. Caflisch,[1] F. Gibou,[1] M. Petersen,[1,3] M. Kang,[1] J. Garcia,[1] and D. D. Vvedensky[1,2,†]
[1]*Department of Mathematics, University of California, Los Angeles, California 90095-1555*
[2]*HRL Laboratories LLC, 3011 Malibu Canyon Road, Malibu, California 90265*
[3]*School of Physics, Georgia Institute of Technology, Atlanta, Georgia 30332*
(Received 23 May 2001; revised manuscript received 13 December 2001; published 19 April 2002)

A level-set model for the simulation of epitaxial growth is described. In this model, the motion of island boundaries of discrete atomic layers is determined by the time evolution of a continuous level-set function φ. The adatom concentration is treated in a mean-field manner. We use this model to systematically examine the importance of various fluctuations in the submonolayer and multilayer regimes. We find that, in the submonolayer regime for large values of D/F, the dominant fluctuations are associated with the spatial seeding of islands. We also show how different microscopic mechanisms can be included into this formalism. In the multilayer regime, our model exhibits surface roughening.

DOI: 10.1103/PhysRevB.65.195403 PACS number(s): 68.55.Jk, 68.35.Bs, 68.35.Fx

I. INTRODUCTION

Epitaxial growth and many other phenomena of practical interest in materials sciences occur on time and length scales that span many orders of magnitude. The most basic physical processes that occur during epitaxial growth occur on the atomic scale, i.e., on length scales of the order of Ångstroms, and time scales that reflect the typical atomic vibration frequencies (i.e., 10^{-13} s). On the other hand, a typical optoelectronic device might be up to several microns in size, and its growth can take minutes or even hours. Thus, modeling epitaxial growth presents an enormous challenge to theoretical physicists and material scientists. Moreover, some of the phenomena that occur during epitaxial growth are inherently stochastic in nature, and an ideal model would seamlessly combine the different time and length scales, but include only the neccessary fluctuations.

The models that are typically used to describe epitaxial growth are either completely stochastic or completely deterministic. Mean-field rate equations that were introduced to this problem[1] almost 30 years ago are a set of coupled ordinary differential equations. They are easy to formulate and easy to solve. The density of adatoms n_1 and of islands of size s, n_s, are given by equations of motion of the form

$$\frac{dn_1}{dt} = F - 2D\sigma_1 n_1^2 - Dn_1 \sum_{s>1} \sigma_s n_s, \tag{1}$$

$$\frac{dn_s}{dt} = Dn_1(\sigma_{s-1} n_{s-1} - \sigma_s n_s) \quad \text{for all } s>1, \tag{2}$$

where F is the deposition flux, D is the surface diffusion constant, and the σ_s are the so-called capture numbers for islands of size s. However, these equations contain no spatial information, and thus do not readily yield information on surface morphology. Moreover, the physical meaning of the input parameters in terms of the underlying atomistic processes is often unclear. In spite of these drawbacks, several results of nucleation theory have been successful in elucidating basic aspects of epitaxial growth. In particular, scaling results derived from nucleation theory can, under the appropriate circumstances, be used to deduce microscopic parameters such as diffusion constants from experimental measurements.[2] But it has also been shown that the simplicity of such a model together with the lack of spatial information has also led to some incorrect interpretations of experimental data.[3]

Continuum models based on partial differential equations (PDE's) are appropriate mainly at large time and length scales.[4,5] By construction, features on the atomic scale are neglected, so they are poorly suited to describe growth on this scale. However, since continuum models as well as rate equations, are based on differential equations, they are amenable to analytic treatments that can elucidate, e.g., asymptotic or stability properties.

An alternative to the completely analytic approaches are atomistic models that explicitly take into account the stochastic nature of each microscopic process that may occur during epitaxial growth. They are typically implemented in the form of molecular-dynamics (MD) (Ref. 6) or kinetic Monte Carlo (KMC) (Ref. 7) simulations. While MD simulations are very useful for identifying relevant microscopic processes, their time and size limitations make them unfeasible for studying epitaxial growth on technologically relevant time and length scales. KMC simulations, on the other hand, have been used successfully to study qualitative, and in limited cases, quantitative, behavior of growth. They allow for easy implementation of a large number of microscopic processes, whose rates are ideally obtained from first-principles calculations.[8] However, the occurrence of very fast rates (which is particularly relevant at higher temperatures) ultimately limits the applicability of these methods to larger systems.

Previously, we have introduced a model to describe epitaxial growth,[9,10] the island dynamics model, that might be considered a hybrid model between continuum, PDE-based methods, and atomistic, stochastic methods. The numerical solution of the model is based on the level-set method,[11,12] which is a general technique for simulating the motion of moving boundaries. This model allows us to describe epitaxial growth as continuous in the plane of the surface, yet it also allows us to discretely resolve each atomic layer.[13]

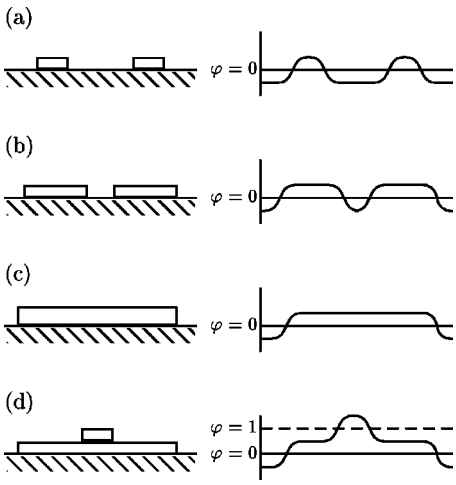

FIG. 1. A schematic representation of the level-set formalism. Shown are island morphologies (left side), and the level-set function φ (right side) that represents this morphology.

Moreover, different sources of fluctuations can be isolated and studied individually.[14] It is the aim of this paper to describe in detail the model, justify its approximations, and present results.

This paper is organized as follows. In Sec. II, the details of the model are presented. In particular, we will explain and justify some of the approximations and choices that are made. In Sec. III, results for the submonolayer growth regime will be discussed. We then describe how additional atomistic processes can be included in our model in Sec. IV. Results that pertain to the multilayer growth regime will be given in Sec. V. Finally, we will discuss the relevance of this model and its implications for modeling epitaxial growth in Sec. VI.

II. THE MODEL

A. Equations of motion and boundary condition

The main component of our model is that a (zero thickness) boundary curve Γ_k, such as the boundary of an island of height $k+1$ can be represented by the set $\varphi=k$, called the *level set*, of a smooth function φ, called the *level-set function*. The boundaries of islands in the submonolayer regime then correspond to the set of curves $\varphi=0$. A schematic representation of this idea is given in Fig. 1, where two islands on a substrate are shown. Growth of these islands is described by a smooth evolution of the function φ [cf. Figs. 1(a) and 1(b)]. The boundary curve $\Gamma(t)$ generally has several disjoint pieces that may evolve so as to merge [Fig. 1(c)] or split.

For a given boundary, the level-set function φ evolves according to

$$\frac{\partial\varphi}{\partial t}+\mathbf{v}\cdot\nabla\varphi=0, \tag{3}$$

where $\mathbf{v}$ is the boundary velocity. The normal component of the velocity $v_n=\mathbf{n}\cdot\mathbf{v}$ contains all the physical information of the simulated system, where $\mathbf{n}$ is the outward normal of the moving boundary and $\mathbf{v}\cdot\nabla\varphi=v_n|\nabla\varphi|$. The boundary velocity is computed by solving the diffusion equation for the adatom concentration ρ

$$\frac{\partial\rho}{\partial t}=F+D\nabla^2\rho-2\frac{dN}{dt}, \tag{4}$$

where F is the deposition flux, D is the surface diffusion constant, and the last term on the right-hand side is the rate of nucleation of new islands on the surface. The velocity of the island boundaries is determined by the flux of adatoms to the island boundaries, and is given by

$$v_n=a^2D(\mathbf{n}\cdot\nabla\rho^- -\mathbf{n}\cdot\nabla\rho^+). \tag{5}$$

The superscripts $(+)$ and $(-)$ label the contributions from above and below the island boundary, and a is the lattice constant. With expression (5) the shape of the islands is essentially circular, but it is easy to alter it to change the shape of the islands. For example, it was shown that the velocity can be modified to obtain square[13] or triangular[10] island shapes to mimic an underlying cubic or triangular lattice structure. All the data shown in this paper are for circular islands, but we have checked that they are essentially the same for square islands.[15] Possible modifications to Eq. (5) that effectively describe other microscopic processes such as edge diffusion or detachment will be discussed later.

In order to solve the diffusion equation (4), a boundary condition needs to be specified. For the case of irreversible aggregation, in which all atoms are adsorbed by the boundary, the standard continuum (absorbing) boundary condition is

$$\rho(\mathbf{x},t)=0 \quad \text{for all } \mathbf{x} \quad \text{with } \varphi(\mathbf{x},t)=0,1,2,\ldots. \tag{6}$$

We will show below, however, that this boundary condition is only valid in the limit $D/F\to\infty$. Otherwise, it needs to be corrected such that $\rho=0$ in a region around the island boundary that is (at least) one lattice constant wide.[16] The solution to the level-set function and the adatom concentration are both obtained on a numerical grid with $n\times n$ grid points that represents a physical substrate of size $L\times L$. Details of the numerical implementation have been given elsewhere.[13]

B. Time dependence of island densities

For the case of irreversible aggregation, a dimer (consisting of two atoms) is the smallest stable island, and the nucleation rate is

$$\frac{dN_{\text{nuc}}}{dt}=D\sigma_1\langle\rho^2\rangle, \tag{7}$$

where $\langle\cdot\rangle$ denotes the spatial average of $\rho(\mathbf{x},t)^2$ and

$$\sigma_1=\frac{4\pi}{\ln[(1/\alpha)\langle\rho\rangle D/F]} \tag{8}$$

is the adatom capture number.[1,17] Please note that the nucleation density N_{nuc} is slightly larger than the island density N, and that the two only agree before coalescence. The param-

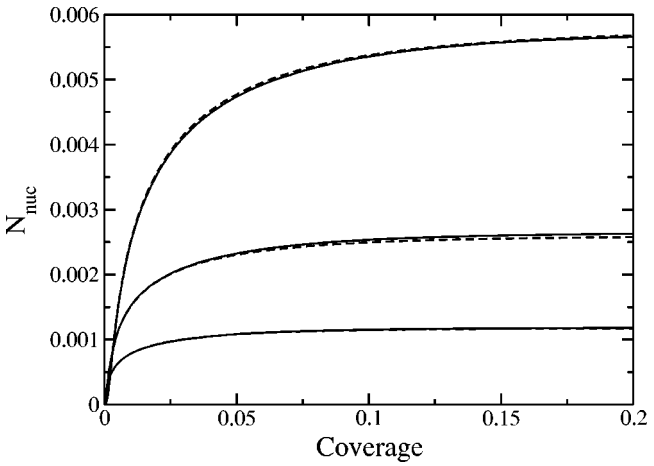

FIG. 2. Nucleation densities as a function of coverage obtained from KMC simulations. The dashed lines are island densities obtained by integrating the adatom density given by the simulations using Eq. (7), the solid lines are the actual number of islands. The three sets of curves are for $D/F=10^5$ (highest densities), $D/F=10^6$ (intermediate) and $D/F=10^7$ (lowest). The simulation data represents averages over eight lattices of size $L=1500$.

eter α reflects the island shape, and $\alpha \simeq 1$ for compact islands. Expression (7) for the nucleation rate implies that the time of a nucleation event is chosen deterministically. Whenever $N_{\rm nuc}L^2$ passes the next integer value, a new island is nucleated. Numerically, this is realized by raising the level-set function to the next level at a number of grid points chosen to represent a dimer. The choice of the location of the new island is described below.

We have tested carefully the validity of expression (7) with KMC simulations. In our KMC model, adatoms are allowed to diffuse over the surface with a diffusion constant D. Once an adatom reaches an island edge, it can diffuse along the island edge as long as it has only one nearest neighbor, but it is not allowed to detach again. This is done to ensure compact island shapes. Thus, the rate for an atom to move can be written as $D_{\rm edge}=D\exp(-mE_e/k_BT)$, where the environment-dependent parameter $m=0$ for single adatoms, $m=1$ for singly bonded step-edge atoms, and $m=\infty$ for higher coordinated atoms. This KMC model is also used in this paper to validate certain level-set results. More details of the KMC model are given in Refs. 18 and 19.

Figure 2 shows a comparison of the nucleation density $N_{\rm nuc}$ obtained from KMC simulations with calculated island densities that were obtained from integrating Eq. (7) with values for ρ as obtained from the simulation. The agreement between the sets of two curves for different values of D/F is excellent. We note that we obtained best agreement with $\alpha=1.05$ (cf. below) in Eq. (8) for σ_1.

C. Nucleation probability

While the time of nucleation is chosen deterministically, the model allows for a stochastic choice of *where* to position new islands. For a fixed geometry, the nucleation event statistics are fully specified by the distribution function $P(\mathbf{x},t)$, the probability density that the next island nucleates at point $\mathbf{x}$ at time t. If this distribution function were known for every configuration of islands that arises in, e.g., a KMC simulation, then by selecting the next nucleation event properly from this distribution in a level-set simulation, the ensemble-averaged island statistics would be exactly the same as those produced by the KMC simulation. The problem, of course, is that this distribution function is not known, and therefore an assumption must be made. There is a clear choice, however. Because the adatom density is extremely low in an ensemble-averaged sense, we would expect the probability of nucleation to be proportional to $\rho(\mathbf{x},t)^2$, the square of the local (spatially dependent) adatom density that is determined by Eq. (4). We refer to this nucleation scheme as probabilistic seeding.

We have tested this assumption using KMC simulations in two artificial, but representative, geometries. The first geometry is a square lattice of size L with periodic boundary conditions in one direction and a perfect sink for adatoms along the remaining two boundaries. The other geometry is a square lattice with periodic boundary conditions in all directions and a perfect sink for adatoms at one site at the center of the lattice. This second situation is equivalent to a periodic array of point sinks for adatoms separated by the lattice dimension L. The initial conditions are no adatoms on the lattice at time $t=0$ and a constant flux F of adatoms for all $t>0$. The two geometries correspond to the case of very large (first case) and very small (second case) islands, with the typical situation being in between.

It is impractical to compute the full distribution function $P(\mathbf{x},t)$, since this would require binning the nucleation events that occur at each lattice site in a time interval Δt that is small in comparison to the temporal changes in P. Instead, we have integrated out the time dependence for all $t>0$ to obtain $P(\mathbf{x})$. This is done by running simulations until the time an island nucleates, then stopping. The position at which the island nucleated is recorded and an ensemble average of this quantity over independent simulations is then performed to obtain $P(\mathbf{x})$. This nucleation probability must then be compared to the time-dependent adatom density that is calculated from independent simulations in which the adatoms do not interact. This is equivalent to solving the diffusion equation for the adatom density with the boundary conditions described above and corresponds exactly to the quantity that is calculated in the level-set simulations. We compare the nucleation probability to the adatom density at the time that is assumed for the next nucleation event in the island dynamics model

$$DL^2\int_0^t \sigma_1\langle\rho(x,t)\rangle^2 dt=1, \tag{9}$$

where $\langle\rho(x,t)\rangle$ is again the spatially averaged adatom density.

Figure 3(a) shows the nucleation probability density plotted as a function of the adatom density for the line sink geometry. Each data point corresponds to the average of the nucleation and adatom densities at points x related by the symmetry of the system. The solid lines are a fit to a quadratic function. These data demonstrate clearly that the

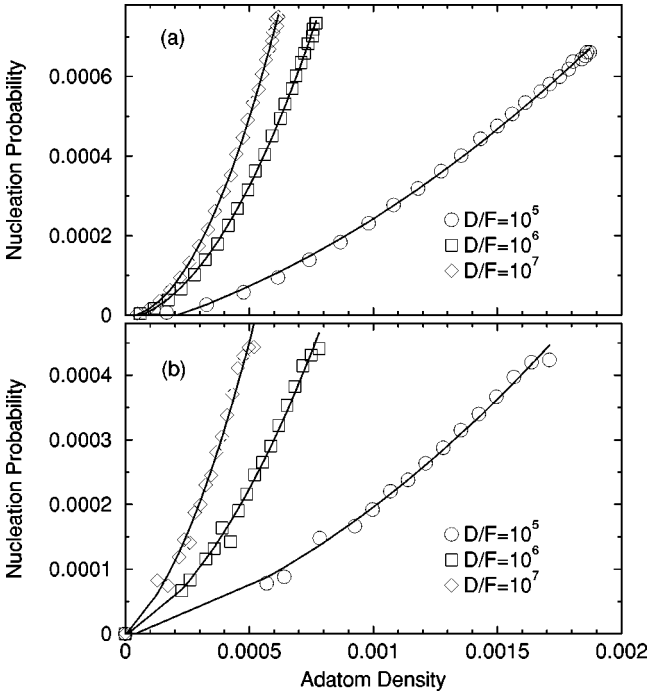

FIG. 3. Nucleation probability as a function of adatom density for KMC simulations with (a) the line sink geometry and (b) the point sink geometry, both with system size $L=50$. Solid lines are fits to a quadratic function. The data represent averages over one million configurations.

ensemble-averaged nucleation probability density is indeed proportional to the square of the local average adatom density for all values of D/F shown. Figure 3(b) shows the same data for the point sink geometry, where similar agreement is found. This indicates that the assumption being used for the placement of nucleated islands in our model is independent of island geometry. Careful examination of the fits to a full quadratic function (i.e., a function including a constant and a linear term) show small deviations from a pure quadratic $[P(\rho)=A\rho^2]$ form. However, these deviations are smaller for larger D/F and also go to zero as the fit is done over successively smaller ranges of ρ. This is not surprising since a pure quadratic form is the expected mean-field result, valid in the limit of low adatom density. We have also compared the nulceation probability to the adatom density at several different times other than the one given above and find that the quadratic dependence on ρ^2 is, in fact, valid over nearly the entire time in which significant nucleation occurs. A very similar methodology has recently been used[20] to investigate the nucleation probability as a function of adatom density for geometries and boundary conditions similar to those described above as well as boundary conditions corresponding to an infinite step-edge barrier. Our results are identical to those found for the case of an adsorbing boundary condition $(\rho=0)$. Castellano and Politi[20] also found that for the case of an infinite step-edge barrier, the correlation between ρ^2 and $P(x)$ breaks down; the physical interpretation for this is not yet clear, and more work would be required for extending our methods to cases with large step-edge barriers.

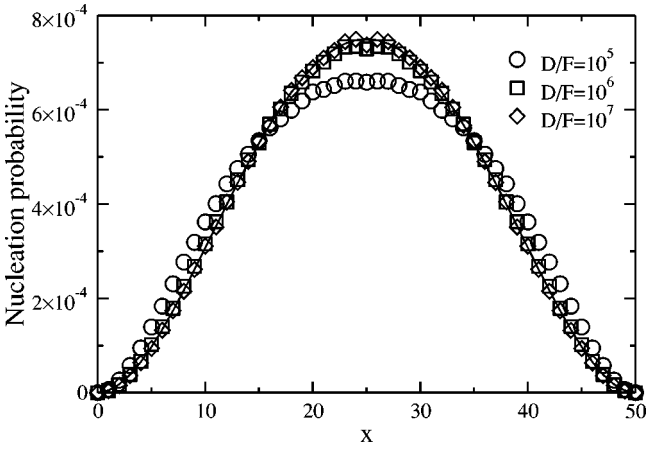

FIG. 4. Nucleation probability as a function of position x for the line sink geometry and system size $L=50$. The circles, squares, and diamonds are simulation data for D/F values 10^5, 10^6, and 10^7, respectively. The solid line is the analytic function $P_0(x)$ as described in the text. The simulation data represent averages over one million configurations.

The first geometry described above allows for an analytic (stationary) solution in the large-L limit:

$$\rho(x)=\frac{F}{2D}x(L-x). \tag{10}$$

This enables us not only to validate the procedure used to perform the corresponding KMC simulations, but also to examine how close the system is to steady state relative to the nulceation time [given by Eq. (9)] and relate this quantitatively to the nucleation probability. Figure 4 shows the nucleation probability density P plotted as a function of position x for the line sink geometry. Also shown (solid line) is $P_0(x)$ obtained from squaring the steady-state adatom density [Eq. (10)] and properly normalizing the distribution. As would be expected, $P_0(x)$ is independent of D/F and the simulation data clearly show that $P(x)$ approaches $P_0(x)$ for large D/F. From this data we conclude that the nucleation probability is independent of D/F as $D/F\rightarrow\infty$ and that the system is very close to the stationary regime for D/F larger than 10^6.

In addition to the probabilistic seeding style, we tested several other seeding styles. The two that have already been discussed in detail in Ref. 14, we refer to as random and deterministic seeding. During random seeding, the location of the new island is chosen completely randomly, without consideration of the value of the adatom concentration. This seeding style might be relevant, for example, when nucleation occurs not because two atoms need to meet, but when (randomly distributed) surface defects act as nucleation centers. In contrast, during deterministic seeding, a new island is always seeded at the position where ρ has its maximum value. One might refer to any seeding style as probabilistic where the probability is weighted with the local value of ρ^p. As p increases, the seeding style becomes progressively more deterministic. Then random seeding corresponds to $p=0$, probabilistic seeding to $p=2$, and deterministic seeding

to $p=\infty$. Results in the submonolayer regime, and in particular results that compare the different seeding styles, will be given in Sec. III.

D. Multilayer growth

We have extended the level-set model to multilayer growth, where the boundaries Γ_k of islands of height $k+1$ are defined by the set of points $\mathbf{x}$, where $\varphi(\mathbf{x},t)=k$ [cf. Fig. 1(d)]. We emphasize that no additional input to the model is needed to describe nucleation in higher layers. When islands are small, the solution of the diffusion equation yields only very small values for the adatom concentration on top of islands. Therefore, for small coverages in layer k, nucleation in layer $k+1$ is negligible. However, as a layer k grows and nears completion, the adatom density on top of layer k increases, leading eventually to nucleation of islands in layer $k+1$. Results in the multilayer growth regime will be discussed in Sec. V. There are indications in the literature[21] that the nucleation rate for islands on top of islands might have a different functional form. However, this seems to be relevant only in the presence of a (large) step-edge barrier. Moreover, our results shown below indicate that the nucleation rate used in our model is correct.

Snapshots of the results from a typical level-set simulation are shown in Fig. 5. Shown is the level-set function [Fig. 5(a)] and the corresponding adatom concentration obtained from solving the diffusion equation (4) [Fig. 5(b)]. The island boundaries that correspond to the integer levels of Fig. 5(a) are shown in Fig. 5(c). Dashed (solid) lines represent the boundaries of islands of height 1 (2). Comparison of Figs. 5(a) and 5(b) illustrates that ρ is indeed zero at the island boundaries (where φ takes an integer value).

III. RESULTS FOR SUBMONOLAYER GROWTH

All the quantitative results presented in this paper will be compared to results from a KMC simulation for irreversible aggregation on a cubic lattice.[18,19] This KMC model includes the same physical processes as the level-set model. Adatom deposition and diffusion are simulated with rates F and D that have the same physical meaning as described above. In addition, we included fast-edge diffusion in the KMC simulation, where singly bonded step edge atoms diffuse along the step edge of an island with a rate D_{edge}.[22] This process has been included to obtain compact islands, since the level-set model leads to compact islands by construction.

A. Island densities

During growth of the first monolayer on a clean substrate, it is possible to distinguish between the nucleation phase, the growth or aggregation phase, and the coalescence phase.[23] The regimes before coalescence are also often collectively called the regime of submonolayer growth. The submonolayer growth regime has been the focus of a large number of studies. One reason is that it is simpler to study this growth regime compared to the multilayer growth regime, as complications and additional effects due to coalescence and roughening are not relevant. Moreover, many morphological features of relevance in the multilayer growth regime are connected to the morphology in the submonolayer growth regime and atomistic processes reveal themselves in the statistics of island sizes and morphologies.

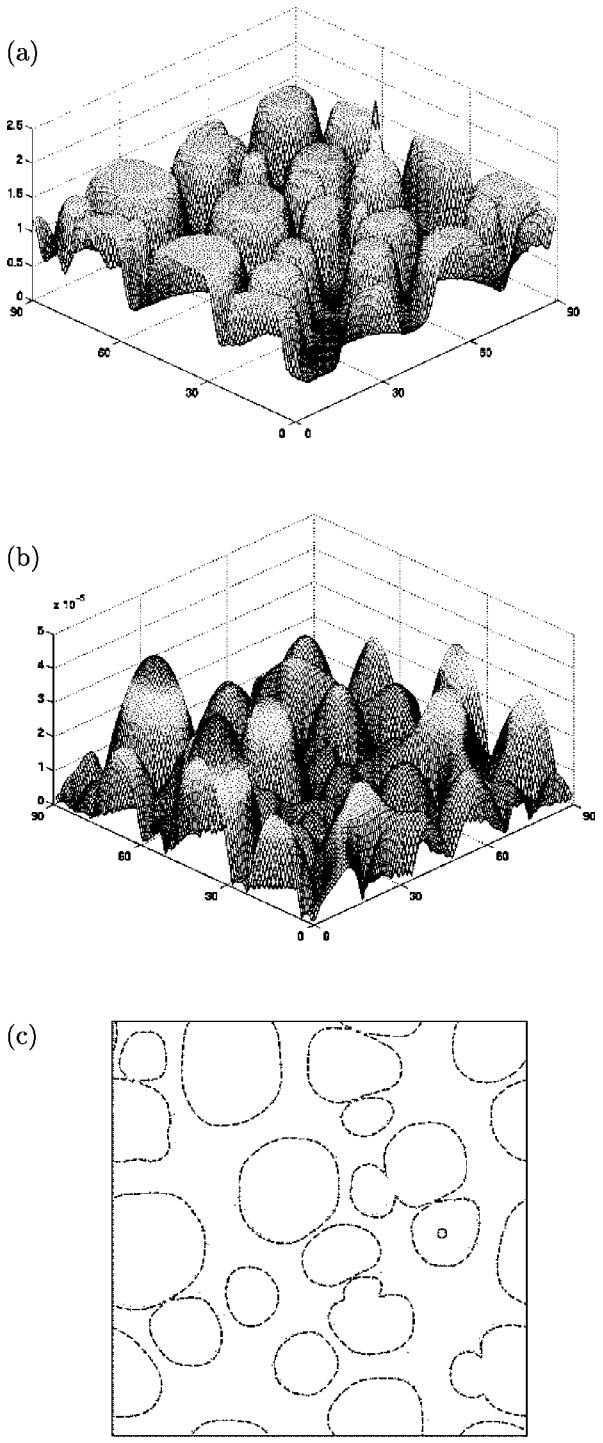

FIG. 5. Snapshots of a typical level-set simulation. Shown are a 3D view of the level-set function (a) and the corresponding adatom concentration (b). The island boundaries as determined from the integer levels in (a) are shown in (c), where dashed (solid) lines correspond to islands of height 1 (2).

We therefore start the discussion of the results of our level-set method by focusing on the submonolayer growth

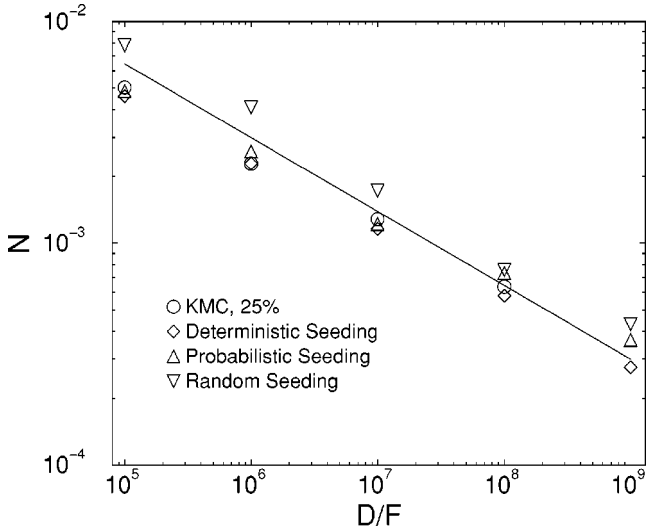

FIG. 6. Log-log plot of the island density N as a function of D/F for the different seeding styles in comparison with data obtained from a KMC simulation.

regime. It is known[1] that for irreversible aggregation, the number density of islands scales according to

$$N \simeq (D/F)^{-1/3}. \tag{11}$$

The island density N is shown in Fig. 6 as a function of D/F obtained with our model with probabilistic seeding, as well as with random and deterministic seeding. All data exhibit the expected scaling behavior. While the data obtained with random seeding is slightly larger, the probabilistic and deterministic seeding style are essentially indistinguishable from each other. However, a detailed comparison of the time evolution of the island densities reveals that there are systematic differences between the different seeding styles. This can be seen in Fig. 7, where the island density N as a function of coverage Θ is shown for $D/F=10^6$. The qualitative dependence on the seeding style for different values of D/F is similar. During random seeding, the number of islands is the

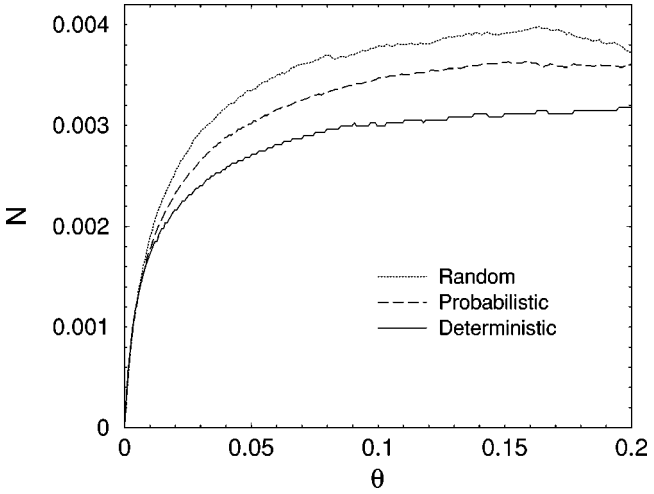

FIG. 7. Time evolution of the island densities N obtained with the different seeding styles for $D/F=10^6$.

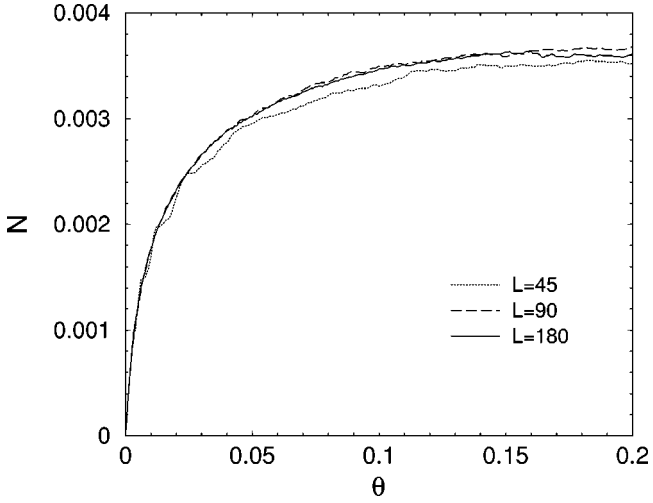

FIG. 8. Time evolution of the island density N for different system sizes with $D/F=10^6$.

highest, while during deterministic seeding, the number of islands is the lowest. The explanation for this will become apparent below.

We also note that the island density is converged with respect to the system size for surprisingly small system sizes. In Fig. 8, we show results of the time evolution of island densities for $D/F=10^6$ obtained with different system sizes. Clearly, the result is essentially unchanged for the island densities for systems of size larger than 90. This is very different than the behavior observed in KMC simulations, where convergence is only reached at much larger system sizes.[24] We speculate that this behavior is an effect of the mean-field treatment of the adatoms, which will be discussed in more detail in Sec. VI. It justifies our choice of the relatively small lattice size of $L=180$ for most of the results presented here.

B. Island-size distributions

The island density discussed so far does not provide any spatial information. A quantity that provides a very useful measure of the spatial correlations on the surface is the island-size distribution. It has been shown in many theoretical[25–27] and experimental[28,29] studies that the island-size distribution scales according to

$$n_s = \frac{\Theta}{s_{av}^2} g(s/s_{av}), \tag{12}$$

where n_s is the density of islands of size s, s_{av} is the average island size, and $g(x)$ is a scaling function.

We have shown in Ref. 14 that only the island-size distribution obtained with the probabilistic seeding style agrees with the one obtained from a KMC simulation, and with experimental data for Fe/Fe(001).[28] The size distribution obtained with the random (deterministic) seeding style is significantly broader (narrower). As p increases, the size distribution becomes sharper and narrower. The reason is that with increasing p, the islands are seeded further apart from each other (there are fewer islands in ''unfavorable'' sites) and the lattice is divided more efficiently. This is the reason why the

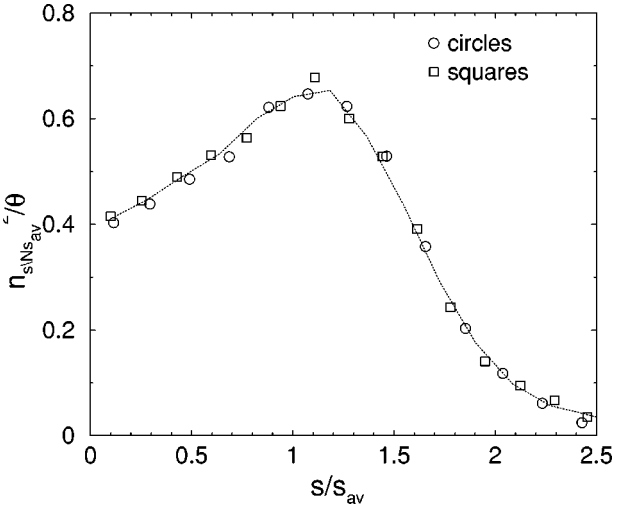

FIG. 9. Scaled island-size distribution for square-shaped and circular islands. Shown is data for a coverage of $\Theta=0.2$ ML and $D/F=10^6$. The dotted line is a guide to the eye.

number of islands decreases as the parameter p increases (cf. Fig. 7). The observation in Fig. 4 that the nucleation probability is always spatially broad, even for large D/F, supports the conclusion that ''deterministic'' nucleation, which would correspond to a delta function for $P(x)$, cannot lead to the correct island size distribution.

We have also tested the effect of the island shape on the size distribution. Figure 9 shows a comparison of the island-size distribution obtained from simulations with circular- and square-shaped islands. It is evident that the size distributions are indistinguishable. The reason is that the distribution of the capture areas is not affected at all by the shape of the islands. As discussed in Ref. 14, it is the distribution of the capture areas that determines the distribution of the island-sizes.

C. Capture numbers

The level-set method as described above gives us an easy way to calculate the capture numbers σ_s that are needed in the rate equations (1), (2). More precisely, the σ_s can be computed by monitoring the rate of aggregation of adatoms to that island. Consider an island of size s with boundary Γ_s. Growth of this island, as described by the velocity v_n, is due to the migration of adatoms toward this island (and subsequent capture). The rate of aggregation of adatoms is then equal to the rate of change in area, which is expressed easily in terms of the level-set function as $\int_{\Gamma_s} v_n d\Gamma_s$. Therefore, the capture number of this island can be expressed as

$$\sigma_s = \frac{\int_{\Gamma_s} v_n d\Gamma_s}{Dn_1}. \tag{13}$$

We emphasize that in our approach each island is allowed to grow in its own environment, and that the spatial extent of the islands is properly taken into account. The results obtained for the capture numbers are shown in Fig. 10. We

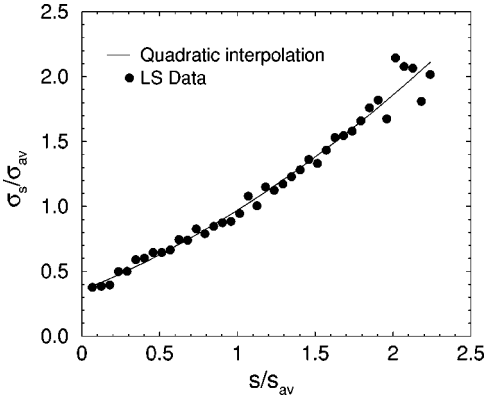

FIG. 10. Capture numbers σ_s as a function of island-size s. The solid line is a quadratic fit to the data with $a=0.134$, $b=0.484$, and $c=0.353$.

observe scaling in coverage Θ and in D/F for the capture numbers as a function of island-size, scaled by their respective averages.[30] Our results suggest that the capture numbers have, as a first approximation, the functional form $\sigma_s = as^2 + bs + c$ (where we obtained the best fit with $a=0.134$, $b=0.484$, and $c=0.353$). The quadratic fit is shown as a solid line in Fig. 10. A similar form was also found in recent work by Amar *et al.*[31] While the quadratic term is small, it is a rather important correction to the linear fit that was previously published.[30] A strict linear dependence of σ_s on s leads to a singularity in the island-size distribution,[32] but a small quadratic correction avoids this singularity. A more detailed analysis of the exact form of the capture numbers can be found elsewhere.[33,34]

The capture numbers and the capture zones are related by[35]

$$\sigma_s \approx \frac{F}{Dn_1} A_s, \tag{14}$$

where A_s is the average area of the capture zones of islands of size s. We have verified that the σ_s as computed by Eq. (13) and as computed by Eq. (14) are indeed in excellent agreement.[30]

One can now integrate the rate equations (1), (2) with the capture numbers that are shown in Fig. 10. It was shown in Ref. 32 that the resulting island-size distribution is in excellent agreement with one obtained from the original level-set simulation. It is essentially indistinguishable from the one shown in Fig. 9. Thus, our level-set approach provides some important information that is needed in the quest for incorporating spatial information in the parameters of a mean-field approach that is based on rate equations.[30]

D. Atomistic effects in boundary conditions

At last, we would like to comment on the validity of the boundary condition that $\rho=0$ at the edges of islands. This boundary condition implies that ρ is nonzero anywhere on the surface, except along a one-dimensional line (with no spatial extent) along the island boundaries. This does not take into account that adatoms typically reside on an adsorp-

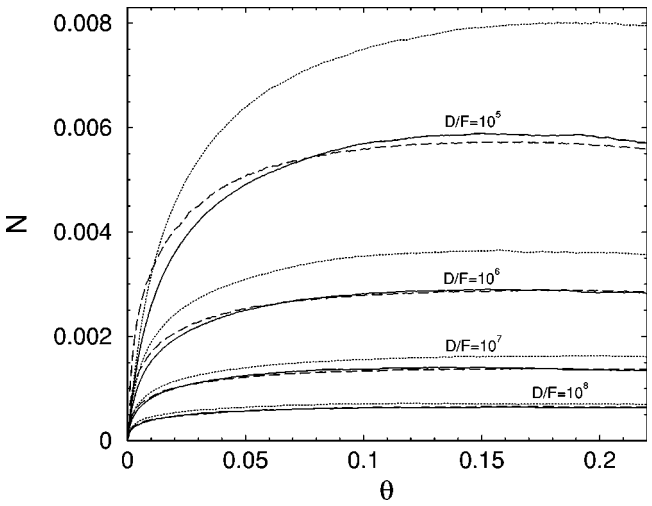

FIG. 11. Island density N for different values of D/F for the boundary condition that includes the discrete size of the atomic lattice constant, as described in the text (solid lines). Data is shown in comparison with KMC results (dashed lines) and results obtained with the original boundary condition (dotted lines).

tion site that has the (lateral) size of the atomic lattice constant a. Thus, there cannot be an adatom next to the island boundary within a distance a, since this atom would be part of the island. Neglecting the spatial extent of this boundary region is a reasonable approximation in a true continuum picture, where the width of such a boundary region is small compared to the larger features such as islands and terraces. For growth on a singular surface under typical growth conditions, however, the average (lateral) size of an island is only 1 to 2 orders of magnitude larger than an atom. Thus, the spatial extent of the boundary region might not be negligible.

We have tested the effect of the discrete size of the boundary region by implementing a boundary condition, where $\rho = 0$ in a region around each island that has width a.[16] Atoms that would be deposited within this boundary region are added to the velocity of the island boundary (to ensure mass conservation). The width of the boundary region might even be larger than a, as there are kinks and defects along a step edge. But a choice of a is appropriate for very compact islands, which corresponds to the case of fast-edge diffusion. The island density obtained from this model is shown in Fig. 11 in comparison to the original model, and also in comparison to results obtained from KMC simulations. The new results agree very well with those obtained from the KMC simulations. The absolute values for N are smaller with the new boundary condition. The reason is that there is now a significant fraction of the surface where $\rho = 0$. As a result, the nucleation rate, and hence the island density N, decreases.

These results indicate that under typical growth conditions the size of the boundary region should not be neglected in *quantitative* studies; for *qualitative* behavior, however, the original boundary condition as given by Eq. (6) and typically used in continuum models is fine. The difference between the two boundary conditions becomes smaller as D/F increases. The reason is simply that the relative importance of the boundary region decreases, because the average island-size increases. Thus, in the limit of $D/F \to \infty$, we reach the continuum limit where the effects of the discrete size of the lattice constant can be neglected. We have also looked at the island-size distribution obtained with this improved boundary condition. It is not shown here, but is indistinguishable from the one shown in Fig. 9.

Finally, we would like to make the following observation. In order to get best agreement in a comparison of the actual island density with the integrated island density (cf. Fig. 2), we chose $\alpha = 1.05$ in Eq. (8). A physical interpretation of α can be found in Ref. 17, where the radius of an island and the square root of its size are related through α. This correction that leads to an effective radius was introduced to mimic anisotropic island shapes. For an island with radius $20a$, $\alpha = 1.05$ implies that an effective island boundary is offset by a, the atomic lattice constant. For $D/F = 10^6$ the average interisland spacing is approximately $20a$ in the precoalescence regime. Thus, an alternative interpretation of the effective radius introduced in Ref. 17 is the atomic size effect described in this section.

IV. ADDITIONAL ATOMISTIC PROCESSES

The model and the results discussed so far are valid for irreversible aggregation. In particular, it has been assumed that only one effective microscopic parameter is needed, which is the surface diffusion constant D. This surface diffusion constant might simply be the rate of hopping of an atom from one lattice site to a nearest-neighbor site. It might, however, also be an effective parameter that describes diffusion due to different, competing mechanisms, such as hopping and exchange. As the temperature increases, other microscopic mechanisms might become relevant, which can easily be incorporated into our level-set framework. Here, we discuss briefly three mechanisms referred to as edge diffusion, diffusion over a step edge (often called Ehrlich-Schwoebel barrier[36]), and detachment of atoms from a step edge.

In a discrete, atomistic method, single (''complete'') atoms are attached to selected sites at certain time steps. In the absence of edge diffusion, this attachment of isolated step-edge atoms creates an instability, which is then the origin for fractal-like growth. In such atomistic models, and for many real systems, it can be surpressed by edge diffusion. More precisely, edge diffusion surpresses the onset of an instability until the length of a step edge is comparable to an edge diffusion length. This is in contrast to our model, where a fraction of an atom is attached to every site along the island boundary at every time step. Without island-island correlation, and without numerical effects, an island would, therefore, never become unstable and grow ''fingers.'' Thus, the mean-field treatment of the adatoms in our level-set method can be interpreted as effectively capturing edge diffusion. In practice, our model also develops instabilities that lead to fingering because of numerical instabilities and island-island correlations. But these instabilities develop on a very different time and length scale than in a discrete, atomistic model.

In particular, the size of the fingers and the time when they start developing is determined by the numerical resolution n/L of the physical system, while in an atomistic model the width of the fractal fingers is intimately connected to the atomic size and the value of edge diffusion.

However, there is no mechanism in our model that provides for smoothing of the island edges after the coalescence of islands. It has been shown in a number of studies that edge diffusion has a pronounced effect on the roughening transition in the multilayer growth regime.[37,38] Therefore, it is important to incorporate edge diffusion into the model, and we modified the expression for the velocity in our model to

$$v_n = a^2 D(\mathbf{n}\cdot\nabla\rho^- - \mathbf{n}\cdot\nabla\rho^+) + D_{\text{edge}}(\kappa - \kappa_{av}), \quad (15)$$

where D_{edge} relates to the edge diffusion rate, and κ and κ_{av} are the local and average curvature of the island. We would like to note that we chose a dependence on $\kappa - \kappa_{av}$ instead of a dependence on the second derivative of κ because of numerical efficiency. The expression we chose is conservative, and we believe that during growth it captures the main effects of edge diffusion. The effect of edge diffusion is particularly pronounced in the multilayer growth regime. Results obtained with Eq. (15) for the velocity will, therefore, be discussed below.

Atoms that diffuse toward a step edge might have a barrier for incorporation into the step edge that is different than the diffusion barrier, and also different depending on whether the atom is coming from the terrace above or below the step edge. We note that such an additional step-edge barrier can, in principle, also be included into our model through a modification of the boundary condition, but such a modification has not been considered here.

An atom that attaches to an island boundary gains a certain amount of bond energy. However, if the activation temperature is sufficiently high, it can also detach again from the island boundary. This process is described by a microscopic rate that might be called the detachment rate. Thus, in order to describe within our model epitaxial growth at higher temperatures, or processes close to equilibrium such as island ripening, the detachment rate has to be included into our model. This can be done by adding a (negative) detachment velocity term to the normal velocity v_n. Probably the most important consequence of this process is an eventual breakup of very small clusters (i.e., dimers). The stochastic nature of such breakup events can be accounted for by defining a probability for breakup that is also determined by the detachment rate. A number of additional numerical and modeling challenges need to be considered. Details and results on these extensions will be presented elsewhere.[39]

V. EXTENSION TO MULTILAYER GROWTH

In ideal layer-by-layer growth, a layer is completed before nucleation of a new layer starts. In this case, growth on subsequent layers would essentially be identical to growth on previous layers. In reality, however, nucleation on higher layers starts before the previous layer has been completed and the surface starts to roughen. This roughening transition depends on the growth conditions (i.e., temperature and deposition flux), and the material system (i.e., the value of the microscopic parameters). At the same time, the average lateral feature size increases in higher layers, which we will refer to as coarsening of the surface. This roughening and coarsening can be measured by studying quantities such as the surface roughness, step-edge density, or island density per layer, which will be the focus of this section.

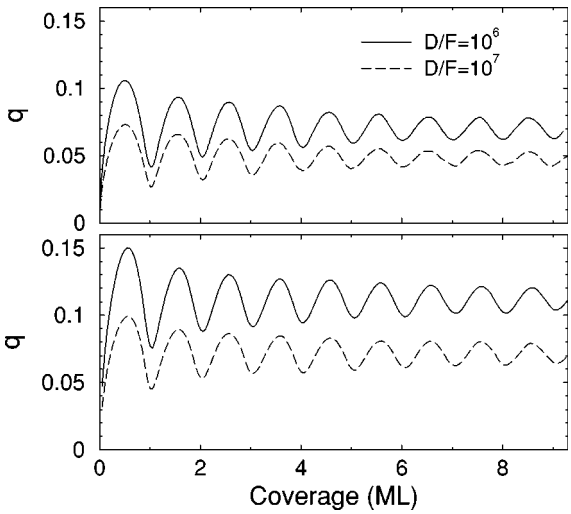

FIG. 12. Oscillations of the step-edge density for different values of D/F obtained with the level-set method (upper panel) and a corresponding KMC simulation (lower panel).

A. Step-edge density

The step-edge density is a good measure to describe the quality of the layer-by-layer growth. Moreover, it is believed to be a good representation of the intensity of the specular reflection high-energy electron-diffraction spot, which is a very common *in situ* sensor during epitaxial growth. In Fig. 12 (upper panel) we show the time evolution of the step-edge density q for different values of D/F, where q is defined as the total length of all the island edges divided by the lattice size. It is evident that q exhibits oscillations, where the period relates to the layer completion time. The absolute value of q depends on D/F, and is highest for lower values of D/F. The reason is that for lower values of D/F, the number of islands on the surface increases (while their size decreases), and as a result the total perimeter of all islands increases. Moreover, we observe that the oscillations decay faster for lower values of D/F. This means that the surface roughens faster for lower values of D/F, as expected.

The values obtained with a corresponding KMC simulation [cf. Fig. 12 (lower panel)] show the same trend as a function of D/F, but the absolute values are 20% to 30% higher than the level-set results. The reason for this is the following. In a KMC simulation, the atomic roughness along a step edge is resolved, while step edges in our island dynamics model are smooth. For example, for an island of size 5×5 that is arranged as a perfect square, there are 20 edge sites. Introduction of just one defect along one step edge (where an atom is removed from a step edge to create a kink pair, and attached somewhere else along the step as a single

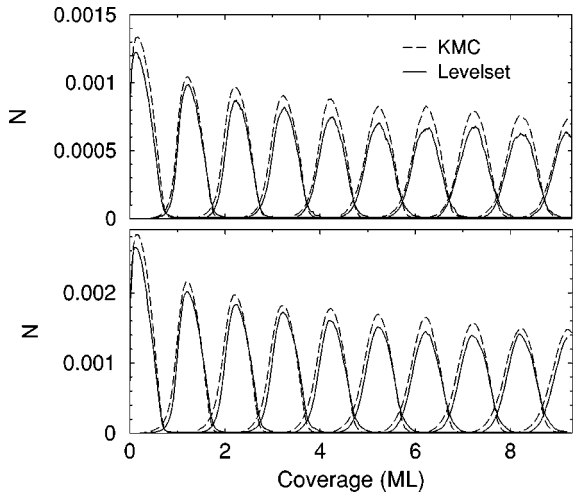

FIG. 13. Island densities N on each layer for $D/F=10^6$ (lower panel) and $D/F=10^7$ (upper panel) obtained with the level-set method and KMC simulations. For each data set there are 20 curves in the plot, corresponding to the 20 layers.

step-edge atom) would then contribute four more step-edge sites, which is an effect of 20%.

B. Layer resolved island density

A more meaningful quantitative comparison that is not sensitive to atomic scale roughness along the step edges is a comparison of the island densities per layer. This is shown in Fig. 13 for two different values of D/F. The KMC results were obtained with a value for the edge diffusion that is 1/100 of the surface diffusion constant. There is no microscopic justification for this value. It was chosen because it provides the best agreement, and because it is known from earlier work that it guarantees essentially smooth step edges.[19] The island density decreases as the film height increases. This and the fact that the maximum roughness increases very little (it essentially does not exceed 0.5 for $D_{\mathrm{edge}}=0$; cf. Fig. 15 and the following section) implies that the film coarsens. This is also evident in Figs. 14(a) and 14(c), where we show typical snapshots of the island morphology after 0.25 [Fig. 14(a)] and 20 layers [Fig. 14(c)] are deposited.

C. Surface roughness

We now focus on the evolution of the surface roughness w, which is defined as

$$w^2=\langle(h_i-\langle h\rangle)^2\rangle, \tag{16}$$

where the index i labels the lattice site. In particular, we will study the effect of edge diffusion, as introduced in Eq. (15), on the roughness evolution. There have been a number of recent atomistic studies[37,38] that show edge diffusion produces an uphill current toward islands, and, as a result, edge diffusion enhances the roughening of the surface. This behavior is somewhat surprising, since one would initially expect that the overall effect of edge diffusion is a smoothing of the surface. It was argued that the underlying mechanism

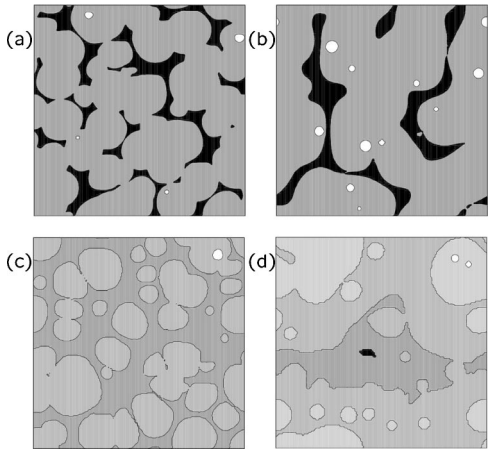

FIG. 14. Snapshots of a typical island dynamics simulation at a coverage of 0.25 monolayer [(a) and (b)], and after 18 layers have been deposited [(c) and (d)]. Shown are results with $D_{\mathrm{edge}}=0$ (left side) and with $D_{\mathrm{edge}}=100$ (right side).

for the roughening is an uphill current that is due to an asymmetry at corners along the step edge. Recent results[19] based on a KMC simulation indicate that there might be an alternative explanation for the enhanced roughening: Faster edge diffusion leads to more compact island shapes, and as a result the residence time of an atom on top of compact islands is extended. This promotes nucleation at earlier times on top of higher layers, and, thus, enhanced roughening. It was suggested that this mechanism is independent of an asymmetry along the step edge.

In Ref. 19 there are still corners and thus asymmetries present along step edges. The level-set method grows smooth step edges, however, so that no corner asymmetries are present in this simulation. Thus, an enhanced roughening with increasing edge diffusion obtained with the level-set method would unambiguously show that the longer residence time of atoms on top of compact islands can lead to enhanced surface roughening. The time evolution of w for different values of D_{edge} is shown in Fig. 15. We clearly see that

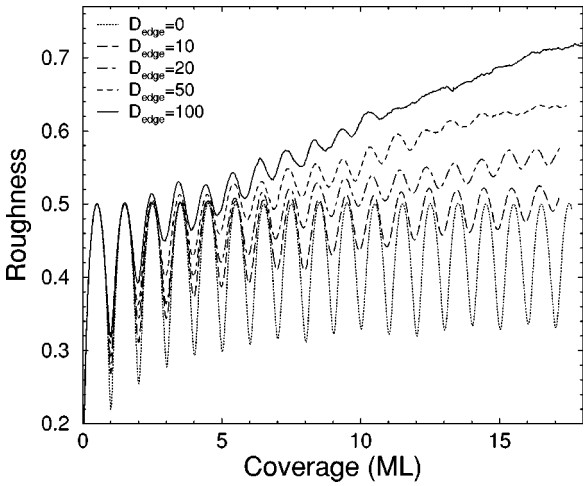

FIG. 15. Time evolution of the surface roughness w for different values of edge diffusion D_{edge}.

the surface roughness increases dramatically as edge diffusion increases. This unexpected behavior is also evident in Fig. 14. Figures 14(b) and 14(d) show a typical surface morphology with the incorporation of edge diffusion at the same times as Figs. 14(a) and 14(c). At early times, there is almost no difference [Figs. 14(a) and 14(b)]. However, at later times [Figs. 14(c) and 14(d)] there are clearly more layers exposed on the surface, in agreement with a larger surface roughness.

We also note that a careful analysis of Fig. 13 reveals that the island densities at higher layers start deviating from zero at earlier times as the film thickens. This also is an indication that the system progressively moves away from the layer-by-layer growth regime, and that the film roughens.

VI. DISCUSSION

We have described the application of the level-set method to a model for epitaxial growth and illustrated our methodology for the submonolayer and multilayer regimes. This approach provides a semianalytic alternative to KMC simulations and is ideally suited to the study of epitaxial phenomena. The main advantages of our method stem from the level-set treatment of boundary motion and, in particular, the topological changes associated with creation (nucleation), motion (growth), and merging (coalescence) of island edges. Moreover, because the lateral coordinates (x,y) are continuous, while the growth direction (z) is discrete, the method can be applied to systems that are large on a lateral scale (up to 1 μm), but are only a few atomic layers thick.

There are three main physical ingredients in our approach that warrant discussion: (i) the implementation of nucleation, (ii) the mean-field description of the adatom field, and (iii) the inclusion of fluctuations. The main input into the level-set equation is an expression for boundary motion. For irreversible aggregation this has two contributions: a source term (i.e., nucleation) and a velocity (i.e., growth). With our treatment of the adatom diffusion field (see below), determining the velocity is a straightforward matter, and the result is given in Eq. (5). Nucleation of new islands, however, is a more delicate matter as it requires specifying both the *times* and *locations* of these events. As described in Sec. II, nucleation times are accounted for by an expression derived from rate equations. But the location of new islands represents a degree of freedom in our approach in that any prescription can be applied, since the resulting spatial distribution of islands is self-consistently accommodated by the corresponding changes in the adatom population. This, in turn, affects the distribution of island-sizes, so the correct choice, as determined by comparisons with KMC simulations or experiments, can be made by varying the nucleation seeding styles. We find that a probabilistic seeding style, weighted by the local value of ρ^2, provides the best agreement. This choice also has implications for the importance of fluctuations in the submonolayer regime, as will be discussed below.

The density of adatoms is described within a mean-field approximation as the solution of a diffusion-type equation with absorbing boundary conditions at island edges. In this sense, our method is intrinsically ''multiscale,'' in that atomistic information about attachment and detachment is incorporated into the boundary conditions at island edges for the continuous adatom field. The validity of our treatment of the adatom diffusion field rests on there being sufficient adatom mobility in comparison to the deposition flux that a coarse graining of the discrete adatom density, as obtained from an ensemble of KMC simulations, is appropriate. Thus, this is effectively an approximation that becomes more accurate as D/F increases, despite the fact that the adatom density decreases accordingly. In the regime $D/F \to 0$, which corresponds to the dominance of flux over adatom diffusion, our approach breaks down as growth occurs mainly by the direct attachment of deposited atoms to island edges.

The preceding discussion highlights how different fluctuations enter into our treatment of various processes. In particular, our results suggest that in the large D/F limit, the only important fluctuations in the submonolayer regime are due to the spatial seeding of islands. Other sources of fluctuations have no effect on the island-size distribution. This result has a number of important implications. Most apparent is that, since the dominant fluctuations are associated with the spatial arrangement of islands, there is no mean-field theory that can capture the form of the distribution of island sizes as D/F becomes large. In other words, the limit of large D/F corresponds to an inherently fluctuation-dominated regime. Moreover, our results show that the nature of these fluctuations influences the form of the distribution function, so the solution to our equations is not unique. The selection of the ''correct'' solution occurs in the nucleation phase which, as $D/F \to \infty$, collapses to an infinitesimal interval near $t=0$, so this effectively corresponds to an ''initial condition.'' This effect is completely beyond the scope of any mean-field approach.

Our final topic on the role of fluctuations concerns the deposition flux. We treat this flux in a mean-field manner that is analogous to that of the adatoms, i.e., a spatially and temporally uniform source for the adatom diffusion field. Although, in the large D/F limit, the fluctuations in the deposition flux are expected to be unimportant in the submonolayer regime of growth, their role in the multilayer regime cannot be neglected. The reason is due to the phenomenon of kinetic roughening.[40] Renormalization-group calculations of the asymptotic roughening of models for epitaxial growth[41,42] indicate that fluctuations in the deposition flux represent a ''relevant'' variable. Thus, the deposition fluctuations eventually dominate the diffusion flux. In the calculations described in Sec. IV, kinetic roughening is observed, but the exponents associated with the surface roughness are expected to be those due to diffusion fluctuations alone,[41] rather than those due to fluctuations in the deposition flux.[42] Physically, the reasons for the observed differences are as follows. In our model, kinetic roughening occurs by the random nucleation of islands according to the rules described above. This is a ''conservative'' process, in that the total mass on the surface does not change, and occurs at a rate proportional to the local value of ρ^2. However, fluctuations in the deposition flux can also cause nucleation by direct impingement onto an adatom. This is a ''nonconservative'' process, since the mass on the surface increases, and

occurs at a rate proportional to the local flux and local adatom density $F\rho$.

We conclude with a discussion of extensions of our approach. We have described a basic model for homoepitaxy on an isotropic substrate. Anisotropy in the substrate can be readily included at the level of surface diffusion and in the attachment rates, the latter through the velocity function.[10] Moreover, the coupling to other external continuous fields can also be carried in this general framework. At every time step, the velocity of all island boundaries is calculated from the integration of a global field. In the work described here, this global field is the adatom diffusion field. The same approach is appropriate, for example, to an elastic field, which can be applied to modeling the strain relaxation in heteroepitaxial systems. More substantial modifications to our basic method may be required to account for the presence of multiple diffusing species. The simplest case, where the effect of the additional species can be subsumed by solving a separate diffusion equation and, possibly, vertical ordering (i.e., a $ABAB\cdots$ layer structure), can be treated within our current framework. However, if there is a lateral ordering with competing phases (e.g., the coexistence of multiple reconstructions on certain semiconductor surfaces) then one must introduce separate level-set functions and corresponding velocity functions for each phase.

ACKNOWLEDGMENTS

The authors acknowledge financial support from NSF and DARPA through cooperative agreement DMS-9615854 as part of the Virtual Integrated Prototyping (VIP) Initiative and from the NSF focused research group Grant DMS-0074152. M.P. acknowledges support from the NSF through Grant No. DMR-953-1115.

*Electronic address: cratsch@math.ucla.edu

†Permanent address: The Blackett Laboratory, Imperial College, London SW7 2BZ, United Kingdom.

[1] J. Venables, Philos. Mag. **27**, 697 (1973).

[2] H. Brune, G.S. Bales, J. Jacobsen, C. Boragno, and K. Kern, Phys. Rev. B **60**, 5991 (1999).

[3] H. Brune, K. Bromann, H. Roder, K. Kern, J. Jacobsen, P. Stoltze, K. Jacobsen, and J. Norskov, Phys. Rev. B **52**, R14 380 (1995); C. Ratsch and M. Scheffler, *ibid.* **58**, 13 163 (1998); K.A. Fichthorn and M. Scheffler, Phys. Rev. Lett. **84**, 5371 (2000); A. Bogicevic, S. Ovesson, P. Hyldgaard, B.L. Lundquist, and D.R. Jennison, *ibid.* **85**, 1919 (2000).

[4] J. Villain, J. Phys. I **1**, 19 (1991).

[5] J. Krug, Adv. Phys. **46**, 139 (1997).

[6] M. Schneider, I. K. Schuller, and A. Rahman, Phys. Rev. B **36**, 1340 (1987); M. H. Grabow and G.H. Gilmer, Surf. Sci. **194**, 333 (1988); B.W. Dodson, CRC Crit. Rev. Solid State Mater. Sci. **16**, 115 (1990).

[7] J. D. Weeks and G. H. Gilmer, Adv. Chem. Phys. **40**, 157 (1979); S. Clarke and D. D. Vvedensky, Phys. Rev. Lett. **58**, 2235 (1987); A. Madhukar and S.V. Ghaisas, CRC Crit. Rev. Solid State Mater. Sci. **14**, 1 (1988); H. C. Kang and W.H. Weinberg, J. Chem. Phys. **90**, 2824 (1989); H. Metiu, Y.-T. Lu, and Z. Y. Zhang, Science **255**, 1088 (1992).

[8] C. Ratsch, P. Ruggerone, and M. Scheffler, in *Surface Diffusion: Atomistic and Collective Processes*, edited by M. C. Tringides (Plenum, New York, 1997), pp. 83–101.

[9] M.F. Gyure, C. Ratsch, B. Merriman, R.E. Caflisch, S. Osher, J.J. Zinck, and D.D. Vvedensky, Phys. Rev. E **58**, R6927 (1998).

[10] R.E. Caflisch, M.F. Gyure, B. Merriman, S. Osher, C. Ratsch, D.D. Vvedensky, and J.J. Zinck, Appl. Math. Lett. **12**, 13 (1999).

[11] S.J. Osher and J.A. Sethian, J. Comput. Phys. **79**, 12 (1988).

[12] S. Chen, B. Merriman, S.J. Osher, and P. Smereka, J. Comput. Phys. **135**, 8 (1997).

[13] S. Chen, B. Merriman, M. Kang, R.E. Caflisch, C. Ratsch, L.-T. Cheng, M. Gyure, R.P. Fedkiw, C. Anderson, and S. Osher, J. Comput. Phys. **167**, 475 (2001).

[14] C. Ratsch, M.F. Gyure, S. Chen, M. Kang, and D.D. Vvedensky, Phys. Rev. B **61**, R10 598 (2000).

[15] We have not checked whether the data presented in Sec. V C is independent of the shape of the island. The reason is that edge diffusion based on curvature would have to be defined differently for square islands.

[16] C. Ratsch, M. Kang, and R.E. Caflisch, Phys. Rev. E **64**, 020601 (2001).

[17] G.S. Bales and D.C. Chrzan, Phys. Rev. B **50**, 6057 (1994).

[18] R.S. Ross and M.F. Gyure, Phys. Rev. B **61**, 8602 (2000).

[19] C. Ratsch, M.C. Wheeler, and M.F. Gyure, Phys. Rev. B **62**, 12 636 (2000).

[20] C. Castellano and P. Politi, Phys. Rev. Lett. **87**, 056102 (2001).

[21] J. Krug, P. Politi, and T. Michely, Phys. Rev. B **61**, 14 037 (2000).

[22] Edge diffusion is not allowed for dimers and trimers. This is done to avoid the indirect diffusion of small clusters. The importance of small cluster diffusion due to fast edge diffusion has been shown in Ref. 21.

[23] J.G. Amar, F. Family, and P.-M. Lam, Thin Solid Films **272**, 208 (1996).

[24] M. Schroeder and D.E. Wolf, Phys. Rev. Lett. **74**, 2062 (1995).

[25] F. Family, P. Meakin, and T. Vicsek, J. Chem. Phys. **83**, 4144 (1985).

[26] M.C. Bartelt and J.W. Evans, Phys. Rev. B **46**, 12 675 (1992).

[27] C. Ratsch, P. Šmilauer, A. Zangwill, and D.D. Vvendensky, Surf. Sci. **329**, L599 (1995).

[28] J.A. Stroscio and D.T. Pierce, Phys. Rev. B **49**, 8522 (1994).

[29] A.R. Avery, H.T. Dobbs, D.M. Holmes, B.A. Joyce, and D.D. Vvedensky, Phys. Rev. Lett. **79**, 3938 (1997).

[30] F. Gibou, C. Ratsch, S. Chen, M.F. Gyure, and R.E. Caflisch, Phys. Rev. B **63**, 115401 (2001).

[31] J.G. Amar, M.N. Popescu, and F. Family, Phys. Rev. Lett. **86**, 3092 (2001).

[32] D.D. Vvedensky, Phys. Rev. B **62**, 15 435 (2000).

[33] F. Gibou, Ph.D. thesis, UCLA (2001).

[34] F. Gibou, C. Ratsch, and R. E. Caflisch (unpublished).

[35] M.C. Bartelt and J.W. Evans, Phys. Rev. B **54**, R17 359 (1996).

[36] G. Ehrlich and F.G. Hudda, J. Chem. Phys. **44**, 1039 (1966); R.L. Schwoebel and E.J. Shipsey, J. Appl. Phys. **37**, 3682 (1966).

[37] M.V. Ramana Murty and B.H. Cooper, Phys. Rev. Lett. **83**, 352 (1999).

[38] O. Pierre-Louis, M.R. D'Orsogna, and T.L. Einstein, Phys. Rev. Lett. **82**, 3661 (1999).
[39] M. Petersen, C. Ratsch, R. E. Caflisch, and A. Zangwill, Phys. Rev. E **64**, 061602 (2001).
[40] A.-L. Barabási and H. E. Stanley, *Fractal Concepts in Surface Growth* (Cambridge University Press, Cambridge, UK, 1995).
[41] T. Sun, H. Guo, and M. Grant, Phys. Rev. A **40**, 6763 (1989).
[42] Z.-W. Lai and S. Das Sarma, Phys. Rev. Lett. **66**, 2348 (1991).